

MODELLING INERTIAL MEASUREMENT UNIT ERROR PARAMETERS FOR AN UNMANNED AIR VEHICLE

Bağış ALTINÖZ^{1,2}, Hüsamettin EKEN¹, Anıl CÖNGER¹ and Sultan CAN²

¹Roketsan, Ankara, TÜRKİYE

²Ankara University, Faculty of Engineering, Department of Electrical and
Electronics Engineering, Ankara, TÜRKİYE

ABSTRACT. This paper demonstrates a study that focuses on the modeling, design, and realization of an Inertial Measurement Unit (IMU) component for the use of Unmanned Aerial Vehicles (UAV). The experimental data is obtained by multiple flights conducted by the realized UAV (Teknofest–SEMRUK team UAV). The structure is remodeled for increasing the accuracy, and performance of the UAV after the conducted flights. Noise parameters are estimated throughout the Allan variance analysis. MEMS technology-based capacitive-type accelerometers and gyroscopes are preferred. This paper also discusses the error types and compares the real data with the modeled simulation data. Systematic errors of the inertial sensors are simulated according to their datasheet parameters. Sensor filters and noise are modeled and they are also implemented in the simulation. Simulation results and UAV measurements are compared to observe the efficiency of modeling. A complementary filter is presented and combined with a magnetometer, accelerometer, and gyroscope to obtain the ultimate design. The comparison showed a satisfactory agreement among the complementary filter measurements and UAV measurements in the stable position and the results presented.

1. INTRODUCTION

In the last decades, the increment of the demand for tools and equipment that do not involve humans in several application areas increased the studies about Unmanned Aerial Vehicles (UAVs). UAVs are briefly a kind of aircraft that does not have a pilot or passenger, carries equipment suitable for its intended use, such as a camera, GNSS, and laser scanning, and can perform its duty remotely and/or automatically.

Keywords: Complementary filter, inertial measurement unit, sensors, unmanned aerial vehicles.

 bagis.altinoz@roketan.com.tr;  0000-0003-2952-9437

 husamettineec@gmail.com;  0009-0001-2693-4923

 anilconger@gmail.com;  0009-0002-4922-5852

 sultancan@ankara.edu.tr-Corresponding author;  0000-0002-9001-0506.

© 2024 Ankara University

Communications Faculty of Sciences University of Ankara Series A2-A3: Physical Sciences and Engineering

Within the need for automation, the oil and gas industry [1], inspection and control of wind turbines, agriculture, search and rescue, and firefighting applications [2], [3], aerial photography, cargo, and cartography [4], both civil and military [5] - [9] applications are requiring UAVs. Such systems attract a great deal of attention in terms of saving time and cost simultaneously with many tasks. Military, civil (hobby and commercial), and professional use of UAVs for scientific purposes are increasing rapidly in our country and all over the world [10]. Especially in military applications, mission completion in tactical critical military missions without endangering personnel is not only time and cost-saving but also the lifesaving advantage of the UAVs since UAVs find their place in many areas such as intelligence, reconnaissance, attack, early warning, air defense, cargo transportation.

UAV's final design requires several items that should be evaluated individually. As one of the items on the flight control board, one of the most important components is a part of the UAV that can be defined as the brain of the overall system. The control board contains a gyroscope, accelerometer, and magnetometer sensors. The gyroscope sensor is used for measuring angular velocity, the magnetometer is used for direction finding, and the accelerometer sensor is used for acceleration measurement. According to the information received from these sensors, the card provides the desired movement and stabilization by changing the speed of the motors. A development board with an ARM-based processor is used as the control board in the UAV due to features such as power saving and high processing capability. Another crucial element is the engine. In the engine of UAV, brushless electric motors are generally used in RC vehicles because of the need for high KV (revolutions per voltage) and low friction. An electronic speed control card (ESC) is also needed to drive these brushless electric motors used. ESCs are the circuit that defines how fast the motors should spin. To control the UAV manually, at least a 4-channel control and a remote-control receiver that is compatible with this control are needed. Generally, the controls work at 2.4GHz frequency and their antenna lengths are short. For digital communication between the control and the receiver, it is first necessary to make an encrypted match between them. For the UAV to fly, sufficient thrust must be created in the engines. This force is provided by propellers. The propellers to be used in the UAV should be selected in the recommended diameter and structure according to the requirements of the engines. Li-Po batteries must be used to provide the necessary power to these electronic components used in the UAV. By calculating the total electrical power consumption of these electronic components, a battery with the appropriate capacity can be selected for the UAV. Another component is telemetry. With the telemetry module, the UAV can be monitored remotely, either wired or wirelessly. Finally, the GPS module used on the UAV provides the UAV's latitude, longitude, and altitude data according to sea level.

In this study, IMU design as the key component of the UAV is considered and modeled. After the realization of the UAV, the experimental data is obtained by proposed design flights and remodeled to increase the accuracy, and performance of the UAV. A complementary filter is presented and combined with a magnetometer, accelerometer, and gyroscope to obtain the ultimate design. MEMS technology-based capacitive-type accelerometers and gyroscopes are preferred.

2. INERTIAL MEASUREMENT UNIT (IMU) IN UAV DESIGN

Inertial measurement units contain inertial sensors that are generally classified as accelerometers and gyroscopes. IMU integrates multi-axes, accelerometers, gyroscopes, and other sensors for estimating the location of the objects accurately.

Linear accelerations can be measured by accelerometers and angular velocity measurements are made by gyroscopes. Accelerometers are categorized into four different classes in technology viewpoint such as piezoelectric, piezoresistive, capacitive, and quartz accelerometers. Gyroscope technologies are categorized into three branches mechanical, optical, and capacitive. The output of the gyroscopes usually has data in terms of degrees/second. Inertial measurement units containing three accelerometers and three gyroscopes measured with six degrees of freedom. In inertial measurement units, in addition to accelerometers and gyroscopes, there are converters to meet the required power requirement, a processor with which calibration coefficients are loaded, and an interface that provides communication.

Although IMUs are commonly used in navigation the accumulated error is an important drawback that the designers have to cope with since any measurement errors, however small, are accumulated over time. Error is categorized into systematic errors and random errors.

2.1. Systematic Errors. Systematic errors can be defined as errors on inertial sensors they mathematically modeled, calibrated, and generally temperature dependent. Systematic errors occur when the behavior of a component of an inertial sensor changes with temperature. Therefore, the temperature is the primary concern for systematic errors. Decreasing the effect of systematic errors mostly depends on a precise calibration process. Thus, the calibration process must include temperature stabilization. Systematic errors are divided into three different categories: bias, scale factor, and misalignment.

2.2. Bias. Bias, which is also called offset or drift, is one of the systematic error components for inertial sensors. Sources of bias error can be from changes in vibration frequency to different movement electrons in sensor electronics. Bias causes drift in the inertial sensor signal even if a sensor is located at zero input

position or rotation. The unit of bias error is deg/h for gyroscopes mg (milli-g) for accelerometers.

Bias errors in the accelerometer, and gyroscope cause position errors as explained below with Equations (1), (2), and (3):

$$p_a = \int_0^t \int_0^t b_a dt \tag{1}$$

$$p_a = \frac{1}{2} b_a t^2 \tag{2}$$

$$p_g = \int_0^t \frac{1}{2} g b_w t^2 dt = \frac{1}{6} g b_w t^3 \tag{3}$$

where b_a is standing for bias error in the accelerometer, b_g is for bias error in the gyroscope, g , and t are the gravity and time, respectively. p_a is the position error due to the accelerometer bias and p_g is the position error due to the gyroscope bias. An illustration regarding the bias error representation for inertial sensor data is presented in Figure 1.

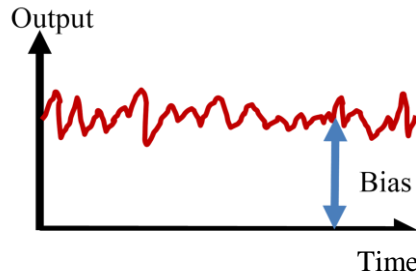


FIGURE 1. Bias Error representation for an inertial sensor data.

2.3. Scale Factor. Ideally, the proportion between input and output is one for the inertial sensors. This ratio is not achievable in most cases. Scale factor error is an essential component in the high acceleration or rotation environment. Because it affects the system in a higher magnitude than bias error. Figure 2 shows three different cases of scale factor error.

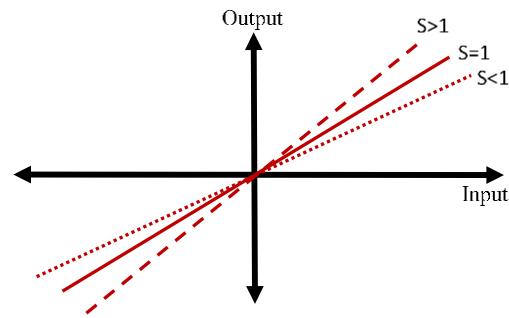


FIGURE 2. Scale Factor error cases for input and input of an inertial sensor.

2.3. **Misalignment.** Sensor alignments are orthogonal in ideal conditions as illustrated in Figure 3. However, integration imperfections, sensor production errors, and coupling between input and output axes are inevitable. Thus, the misalignment error arises.

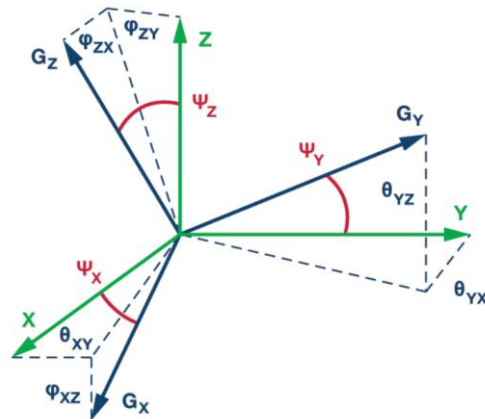


FIGURE 3. Misalignment error between three orthogonal axes.

2.5. **Random Errors.** Inertial sensor measurements include noise as with everything in nature. Random errors can be thought of as the components of noise part of the inertial sensor signals. Random errors differ from each other according to their frequency components. Velocity random walk and angular random walk are white noises for accelerometers and gyroscopes respectively. Additionally, bias instability, flicker noise, and rate random walk are also random errors.

Determining random errors is straightforward because there are two golden methods available in the literature. These methods are power spectral density and Allan variance. The former is generally used in signal and noise analysis, especially for white noise in signal processing applications. The latter is a special tool to estimate random errors on atomic clocks but the same noise parameters affect the inertial sensors. Thus, the same method is used to extract random errors.

In the following sections, angular/velocity random walk and bias instability (or flicker noise) are described.

2.6. Angular/Velocity Random Walk. The most dominant random error parameter is angular and velocity random walk in the inertial sensors. As described before, gyroscope measurement consists of angular random walk, and accelerometer measurements include velocity random walk error. Thermomechanical and electronic noises cause angular/velocity random walk errors. These random errors influence all of the frequency domains. Therefore, these errors are categorized as white noise.

Angular and velocity random walk parameters are estimated by Allan variance analysis. In this study, at least one-hour long data was collected from the inertial sensors to obtain Allan variance graphics. The unit of velocity random walk error is or $\frac{mg}{\sqrt{Hz}}$ and the unit of angular velocity walk is $\frac{deg}{\sqrt{h}}$ or $\frac{deg}{s\sqrt{Hz}}$.

2.7. Bias Instability. common random error parameter because it has low-frequency characteristics. It means that if the effect of bias instability is to be observed, a certain amount of time has to be elapsed after turning on the inertial sensors.

The unit of bias instability for the accelerometer is $\frac{meter}{sec^2}$ or mg , and the unit of bias instability for the gyroscope is $\frac{deg}{h}$ or $\frac{deg}{s\sqrt{Hz}}$. Bias instability error is not modeled in this study because it is not an effective random error parameter for UAV applications.

2.8. Proposed UAV Design and Realization. The mathematical model of the proposed UAV is illustrated in Figure 4 in which there are 6 axes that the UAV can move along.

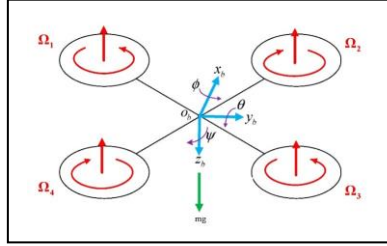


FIGURE 4. UAV configuration for the mathematical model.

$$U1 = b(\Omega_1^2 + \Omega_2^2 + \Omega_3^2 + \Omega_4^2) \quad (4)$$

$$U2 = b \sin\left(\frac{p_i}{4}\right) (\Omega_1^2 - \Omega_2^2 - \Omega_3^2 + \Omega_4^2) \quad (5)$$

$$U3 = b \sin\left(\frac{p_i}{4}\right) (\Omega_1^2 + \Omega_2^2 - \Omega_3^2 - \Omega_4^2) \quad (6)$$

$$U4 = d(\Omega_1^2 - \Omega_2^2 + \Omega_3^2 - \Omega_4^2) \quad (7)$$

The acceleration of yaw-, pitch, and roll angles by combining the engine's moment of inertia and rotor inertia with the equations given above. Obtaining these accelerations is given in the following equations.

$$\ddot{\phi} = \frac{\dot{\theta}\psi(I_{yy} - I_{zz}) + J_r\dot{\theta}\Omega_r + l(U2)}{I_{xx}} \quad (8)$$

$$\ddot{\theta} = \frac{\dot{\phi}\psi(I_{zz} - I_{xx}) - J_r\dot{\phi}\Omega_r + l(U3)}{I_{yy}} \quad (9)$$

$$\ddot{\psi} = \frac{\dot{\theta}\phi(I_{xx} - I_{yy}) + (U4)}{I_{zz}} \quad (10)$$

Likewise, the equations required to obtain the accelerations in the x, y, and z axes are given below.

$$\ddot{X} = \frac{(\sin\Psi\sin\phi - \cos\Psi\sin\theta\cos\phi)U1 - A_x\dot{X}}{m} \quad (11)$$

$$\ddot{Y} = \frac{(\cos\psi\sin\phi + \sin\psi\sin\theta\cos\phi)U1 - A_y\dot{Y}}{m} \quad (12)$$

$$\ddot{Z} = \frac{mg - (\cos\theta\cos\phi)U1 - A_z\dot{Z}}{m} \quad (13)$$

Thus, with these equations given above, it will be possible to simulate a UAV that will fly with command control. The variables required for the equations are given in the table below

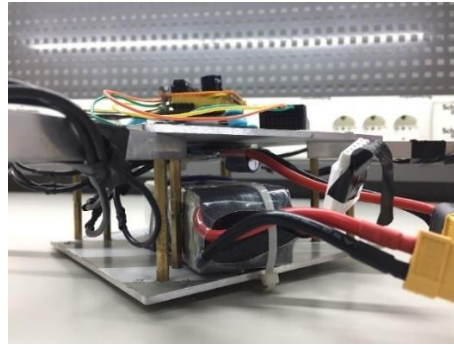
TABLE 1. Variable list for the thrust equations.

Symbol	Description	Unit
I_{xx}, I_{yy}, I_{zz}	Inertia moments	Kgm ²
J_r	Rotor inertia	Kgm ²
l	Rotor axis to quadcopter center distance	m
b	Thrust coefficient	N/s ²
d	Drag coefficient	Nm/s ²
m	Mass of UAV	Kg
A_x, A_y, A_z	Air resistance in each axis	Kg/s

It is also necessary to calculate the total speed of the rotors required for the equations. This total is formed by the difference in the rotation directions of the rotors. In quadcopters, since the first and third motors rotate in the same direction, the second and fourth motors rotate in the same direction, and the total speed is found as follows.

$$\Omega_r = \Omega_1 - \Omega_2 + \Omega_3 - \Omega_4 \quad (14)$$

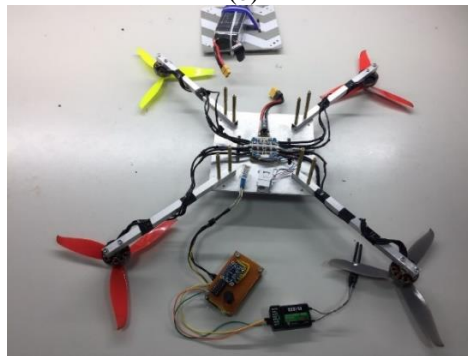
Concerning those calculations and design parameters, the final design is conducted and it is presented in Figure 5. The battery connection, propeller connection, and top view of the design are shown in Figure 5(a), Figure 5(b), and Figure 5(c), respectively.



(a)



(b)



(c)

FIGURE 5. Design a) battery connection b) propeller connection c) top view of the final version.

3. MODELLING AN IMU

To calculate the random walk parameter, it is necessary to retrieve data from inertial sensors at constant temperatures for a long time. After the data are collected, the data is analyzed with the Allan variance method. The Allan variance method examines the data at short time intervals for the first step and then at longer time intervals as the analysis progresses.

The calculation of Allan variance is given below as the averaged data with length $y_i:\tau$, N: data length, and the total number of data with M: τ length.

$$\sigma_{AV}^2 = \frac{1}{2(M-1)} \sum_{i=1}^{M-1} [y_{i+1} - y_i]^2 \tag{15}$$

$$M = \frac{N}{\tau}$$

As a result of the Allan variance calculation, a log-log graph is drawn for different τ lengths as in Figure 6.

Since the most important error parameters in MEMS accelerometers and gyroscopes are the angle and velocity random walk parameters this study focuses on those parameters.

The Angle/Speed random walk parameter is calculated by the intersection of the Allan variance graph and the line with a slope of -1/2. Data were collected for 1 hour from the accelerometers and gyroscopes used within the scope of the project. The resulting Allan variance plots for the gyroscope and accelerometer are shown in Figure 7 and Figure 8, respectively.

Angle and velocity random walking parameters obtained as a result of the tests are given in the table below.

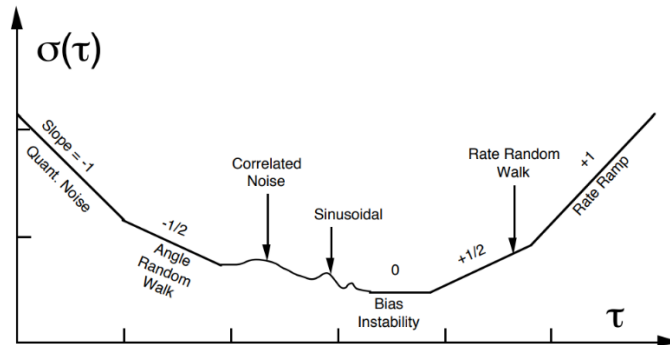


FIGURE 6. Representation of the Allan variance plot for different τ values 0.

TABLE 2. Angle and Speed Random Walk Parameters

Axes	Gyroscope (deg/hr)	Accelerometer ($m/s^2/\sqrt{Hz}$)
X-Axis	1.9368	0.0012
Y-Axis	1.239	0.0012
Z-Axis	1.239	0.0014

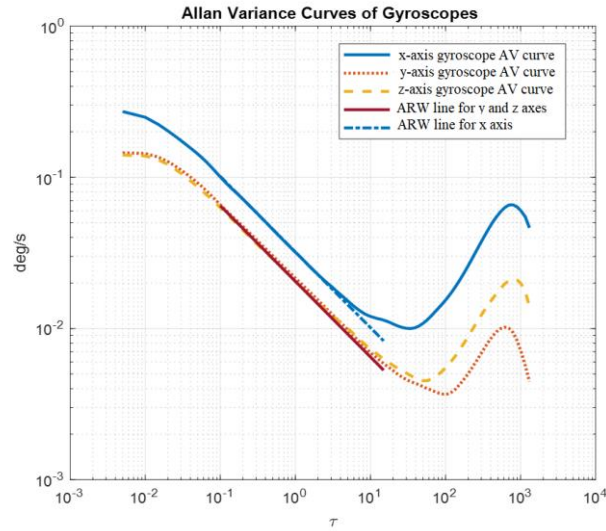


FIGURE 7. Gyroscope Allan variance plot.

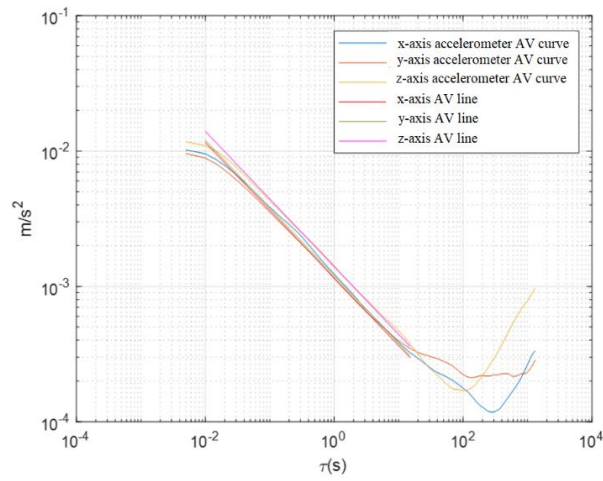


FIGURE 8. Accelerometer Allan variance plot.

While the sensors are being modeled, the filters must also be added to the models simultaneously. To reduce the noise power of the inertial measurement unit, a second-order Butterworth filter with a cutoff frequency of 30 Hz was used. While designing the sensor filter, the values shown in the data file of the sensors were adhered to. The following flow was applied while performing the modeling.

$$y[k] = \frac{N}{\sqrt{\Delta t}} w[k] \quad (16)$$

where N is the angle or noise random walk parameter, $y[k]$ is angle-velocity random walk data, $w[k]$ is white noise, Δt is sampling time. The noise values of the magnetometers used in the inertial measurement unit are taken as a reference. In the fixed position data, the y-axis magnetometer measured 200 microTesla more than the x-axis. While modeling, the relevant value was added directly as a total. A filter with a cutoff frequency of 30 Hz was applied to the magnetometer data.

$$x_m[k] = Aw[k] \text{ and } y_m[k] = Aw[k] + 200uT \quad (17)$$

$y_m[k]$ is standing for magnetometer data y-axis, $x_m[k]$ is magnetometer data x-axis, $w[k]$ is the white noise and A is the magnetometer noise parameter.

3.1. Complementary Filter. The complementary filter method is used widely in the literature, especially in inertial sensor fusion applications. This article uses a basic approach of the complementary filter to obtain the roll, pitch, and yaw angles. Accelerometer and gyroscope measurements are used in roll and pitch measurements. Gyroscope and magnetometer measurements are used in yaw measurements. The weight of the gyroscope measurement to calculate ϕ , θ , and ψ angles is 0.97. Additionally, the weight of accelerometer calculations to ϕ , θ angles is 0.03. Besides, the weight of magnetometer measurements to calculate ψ angle is 0.03. The mathematical equation of the basic complementary filter is given below and the block diagram of the sensor output is shown in Figure 9.

$$o[k] = \alpha(a[k]) + (1 - \alpha)(b[k]) \quad (18)$$

$o[k]$ shows the output of the complementary filter. α is the filter coefficient for sensor a. $1 - \alpha$ is also a coefficient for sensor b. Thus, a basic type of complementary filter is formed.

Comparing the mathematical model output and UAV measurements in the stable position (in zero rotation rate, gravity only affects the z-axis accelerometer) shows that these two measurements fit each other as illustrated from Figure 10 to Figure 15. Figures 10, 11, and 12 illustrate the comparison of UAV measurement and

simulation results of the gyroscope for the x -, y -, and z -axis, respectively. The corresponding comparisons of the accelerometer are shown in Figures 13,14 and 15 for the x -, y -, and z -axis, respectively.

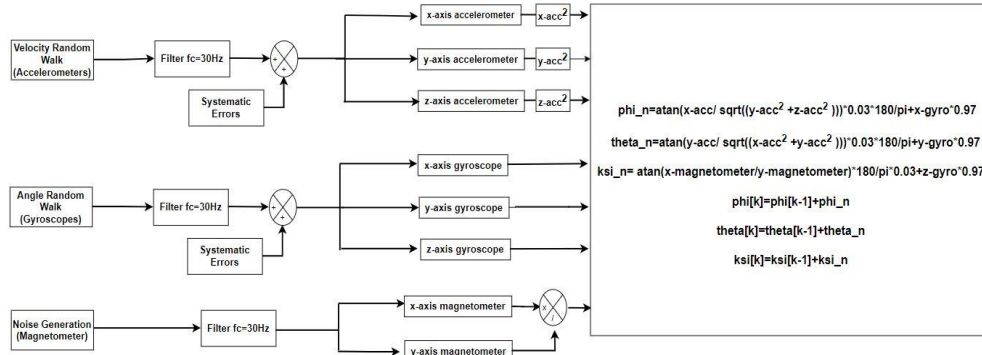


FIGURE 9. Simulink Block for the ultimate design.

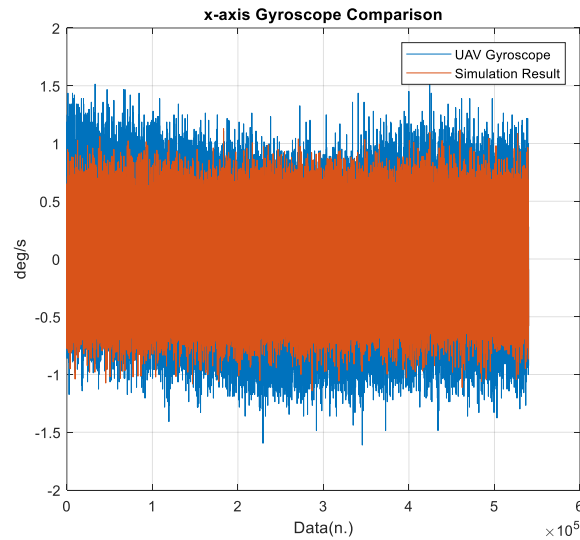


FIGURE 10. Comparison of UAV measurement and simulation result for x-axis gyroscope.

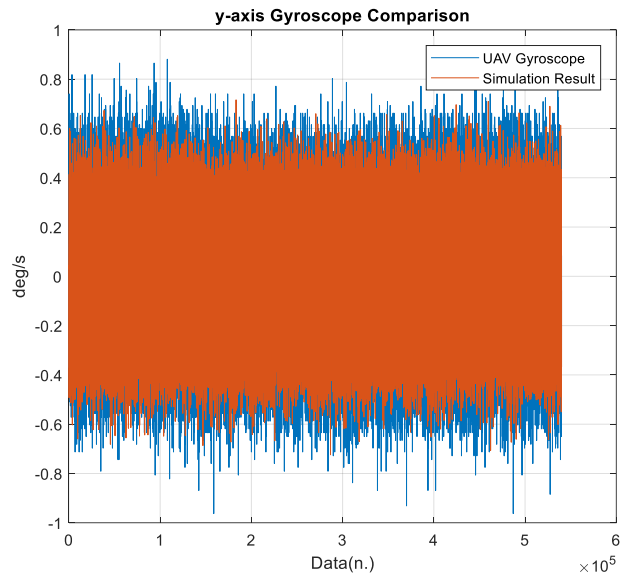


FIGURE 11. Comparison of UAV measurement and simulation result for y-axis gyroscope.

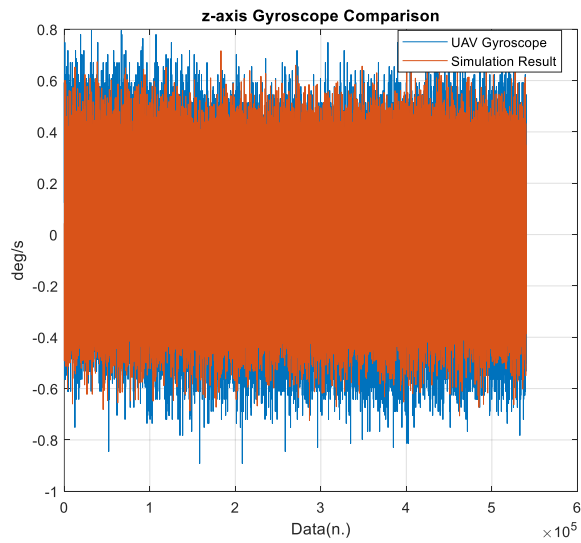


FIGURE 12. Comparison of UAV measurement and simulation result for z-axis gyroscope.

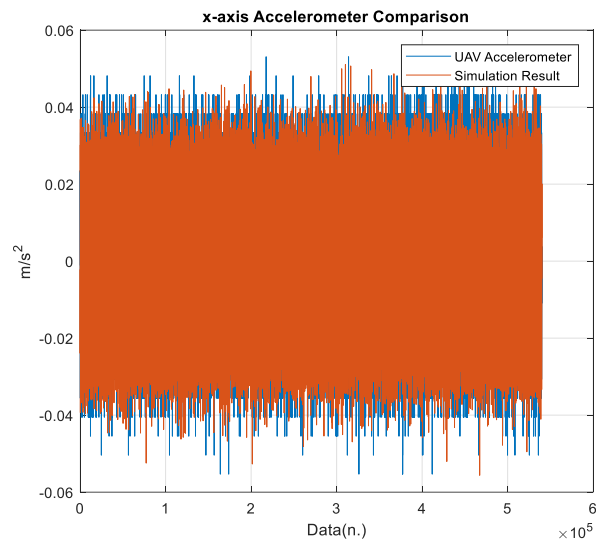


FIGURE 13. Comparison of UAV measurement and simulation result for x-axis accelerometer.

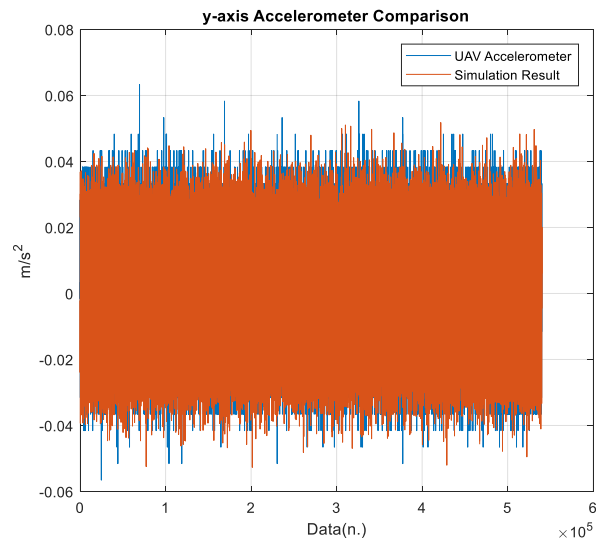


FIGURE 14. Comparison of UAV measurement and simulation result for y-axis accelerometer.

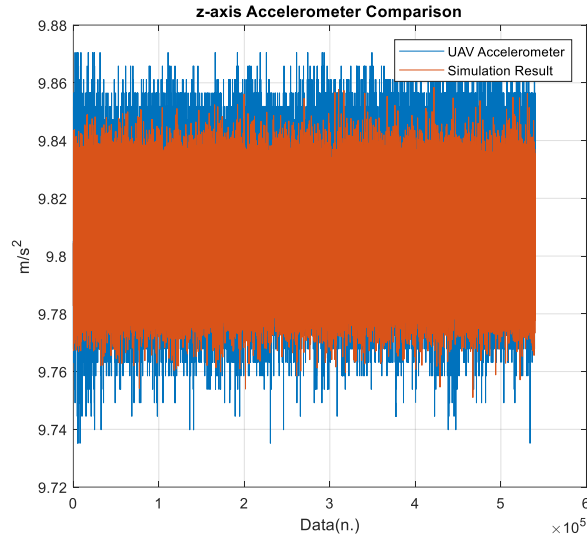


FIGURE 15. Comparison of UAV measurement and simulation result for z-axis accelerometer.

4. RESULTS AND CONCLUSION

This paper has demonstrated the modeling, design, and realization of IMU, which uses MEMS technology-based capacitive-type accelerometers and gyroscopes. The study also discussed the error types by comparing the real data with the simulated one. Remodeling has been performed to increase the accuracy, and the performance, and for this purpose, a complementary filter has been presented and combined with a magnetometer, accelerometer, and gyroscope for obtaining the ultimate design. As a result, in this study;

- Mathematical model of inertial measurement units has been formed and the model has been applied to the UAVs' inertial sensor measurements.
- Noise parameters have been estimated throughout the Allan variance analysis.
- Systematic errors of the inertial sensors have been simulated according to their datasheet parameters.
- Sensor filters and noise have been modeled and they have been also implemented in the simulation. Simulation results and UAV measurements have been compared to observe the efficiency of modeling.
- Magnetic sensors have also been taken into consideration to calculate the heading (yaw angle) of the UAV. Therefore, noise parameters and offset values of magnetic sensors are provided for simulation. Comparing the simulation results and

UAV heading measurements reveals that the suggested model fits the required modeling aspects.

This study can be extended with future works regarding the studies based on different types of gyroscopes and accelerometers instead of MEMS technology-based capacitive-type accelerometers and gyroscopes. Besides, as a future study, the proposed model can be implemented to the low budget, low-accuracy air platforms.

Author Contribution Statements

Bağış Altınöz: Validation, Investigation, Writing-review & editing, Visualization.

Anıl Cönger, Hüsamettin Eken: Investigation, Methodology

Sultan Can: Conceptualization, Writing-original draft, supervision.

Declaration of Competing Interests The authors declare that none of the work reported in this study could have been influenced by any known competing financial interests or personal relationships.

Acknowledgement We gratefully acknowledge the financial support by Scientific Research Projects of Ankara University (BAP) under Grant no 21Ö0443002. We would also like to thank SEMRUK team members and Dr. Tolga İnal for their support and contribution to the Teknofest UAV competition and TUSAŞ lift-up projects.

REFERENCES

- [1] Di Felice, F., Mazzini, A., Di Stefano, G., Romeo, G., Drone high-resolution infrared imaging of the Lusi mud eruption, *Mar. Pet. Geo.*, 90 (2018), 38-51, <https://doi.org/10.1016/j.marpetgeo.2017.10.025>.
- [2] Aydın, B., Selvi, E., Tao, J., Starek, M. J., Use of fire-extinguishing balls for a conceptual system of drone-assisted wildfire fighting, *Drones*, 3 (1) (2019), 17, <https://doi.org/10.3390/drones3010017>.
- [3] Bodnar, L., Restas, A., Qiang, X., Conceptual approach of measuring the professional and economic effectiveness of drone applications supporting forest fire management, *Procedia Eng.*, 211 (2018), 8-17, <https://doi.org/10.1016/j.proeng.2017.12.132>.
- [4] Restas, A., Drone applications for supporting disaster management, *World J. Eng. Technol.*, 3 (2015), 316-321, <https://doi.org/10.4236/wjet.2015.33C047>.
- [5] Rao Mogili, U. M., Deepak, V. L., Review on application of drone systems in precision agriculture, *Procedia Comp. Sci.*, 133 (2018), 502-509, <https://doi.org/10.1016/j.procs.2018.07.063>.
- [6] Marinello, F., Pezzuolo, A., Chiumenti, A., Sartori, L., Technical analysis of unmanned aerial vehicles (drones) for agricultural applications, *Eng. Rural Develop.*, (2016), 15.

- [7] Morey, N. S., Mehere, P. N., Hedaoo, K., Agriculture drone for fertilizers and pesticides spraying, *Int. J. Eng. App. Technol.*, 3 (5) (2017).
- [8] Shaw, I., History of U. S. drones, *Thinking (In) Security, Political Philosophy, and Robots*, (2014), [https://understandingempire.wordpress.com/2-0-a-brief-history-of-u-s-drones/\(2014\)](https://understandingempire.wordpress.com/2-0-a-brief-history-of-u-s-drones/(2014)).
- [9] Stamp, J., Unmanned drones have been around since world war I [Online]. Retrieved from: <http://www.smithsonianmag.com/arts-culture/unmanned-drones-have-been-around-since-world-war-i-16055939/#ZOkewSDbAgEoRHhA.99>.
- [10] Luppicini, R., So, A., A technological review of commercial drone use in the context of governance, ethics, and privacy, *Technol. Soc.*, 46 (2016), 109-119, <https://doi.org/10.1016/j.techsoc.2016.03.003>.
- [11] DigiKey, (2011). Available at: <https://www.digikey.com/en/articles/using-an-accelerometer-for-inclination-sensing>. [Accessed May 2023].
- [12] Allan variance: noise analysis for gyroscopes, (2015). Available at: <https://tele.sens.co/wp-content/uploads/2017/05/AllanVariance5087-1.pdf>. [Accessed May 2023].
- [13] Qi, G., Ma, S., Guo, X., Li, X., Guo, J., High-order differential feedback control for quadrotor UAV: theory and experimentation, *Electronics*, 9 (12) (2020), 2001, <https://doi.org/10.3390/electronics9122001>.
- [14] De Pasquale, G., Soma, A., Reliability testing procedure for MEMS IMUs applied to vibrating environments, *Sensors*, 10 (1) (2010), 456-474, <https://doi.org/10.3390/s100100456>.
- [15] IEEE 952, IEEE standard specification format guide and test procedure for single-axis interferometric fiber optic gyros, (1997), <https://doi.org/110.1109/IEEESTD.1998.86153>.